

# Seeing the unseen in quantum Wigner molecularization in Moiré superlattices

Constantine Yannouleas\* and Uzi Landman†

*School of Physics, Georgia Institute of Technology, Atlanta, Georgia 30332-0430*

(Dated: 19 April 2023)

The few-body problem (with  $N \leq 6$  fermionic charge carriers) in isolated Moiré quantum dots in transition metal dichalcogenide (TMD) superlattices with integral fillings,  $\nu > 1$ , is investigated by employing large-scale configuration interaction (exact-diagonalization) computations, and by performing a comparative analysis of the ensuing first-order (charge densities, CDs) and second-order (conditional probability distributions, CPDs) correlation functions. Our investigations reveal the determining role of the strong inter-particle Coulombic repulsion in bringing about Wigner molecularization, which is associated with many-body physics beyond both that described by the aufbau principle of natural atoms, as well as by the widely used Hubbard model for strongly-interacting condensed-matter systems. In particular, our use of the CPDs brings to light the geometrical polygonal-ring configurations underlying the Wigner molecules (WMs) that remain hidden at the level of a charge-density analysis, apart from the case of  $N = 3$  when a *pinned* WM emerges in the charge density due to the coincidence of the  $C_3$  symmetries associated with both the WM intrinsic geometry and that of the confining TMD potential.

Understanding of the electronic spectral and configurational organization in natural atoms, which played a pivotal role in the early development of quantum mechanics [1, 2], continues to inspire discoveries in research targeting the exploration of the nature of few charged carriers trapped in artificially fabricated, isolated or superlattice-assembled, quantum dots (QDs) [3–5]. Such research aims at utilizing these systems, with high tunability and control, in future quantum information and computational platforms [6–9]. Earlier studies have unveiled formation of quantum Wigner molecules (WMs), originally predicted theoretically [10–34] in two-dimensional (2D) semiconductor QDs, as well as trapped ultracold atoms, and subsequently observed experimentally in GaAs QDs [35–38], Si/SiGe QDs [39], and carbon-nanotubes [40]. Important contributions to this area employed full configuration-interaction (FCI) [17, 18, 23, 25, 29, 30, 34, 41–45] calculations. The FCI treatment goes beyond (1) the central-field Aufbau principle, which underlies the periodic table of natural atoms [46], and (2) the Hubbard modeling of strongly interacting systems [47, 48].

Here such FCI (termed also exact diagonalization methodology) is employed in investigations of few-body fermionic (electrons or holes) Moiré QDs [49–51] in integer-filling transition metal dichalcogenide (TMD) bilayers [52, 53]. Analysis of the strongly-interacting correlated trapped-particles, that extends to second-order correlations, i.e., spin-resolved conditional probability distributions (CPDs, see, e.g., [12, 19, 22, 23, 29, 54]; for the definition, see Eq. (C5) in the Appendix), reveals formation of geometrical polygonal-ring quantum WMs ( $N = 2–6$ ), that remain elusively unseen (hidden) at the level of first-order (charge density, CD; see Eq. (C1) in the Appendix). analysis. Accordingly, a WM spectral or-

dering emerges that contrasts sharply with that expected from both the Hubbard model and the Aufbau principle.

The potential confinement of a 2D TMD Moiré superlattice can be approximated by the expression [55],

$$V(\mathbf{r}) = -2v_0 \sum_{i=1}^3 \cos(\mathbf{G}_i \cdot \mathbf{r} + \phi), \quad (1)$$

where  $\mathbf{G}_i = [(4\pi/\sqrt{3}a_M)(\sin(2\pi i/3), \cos(2\pi i/3))]$  are the Moiré reciprocal lattice vectors.

For angles  $\phi < 40^\circ$ , the attractive pockets of  $V(\mathbf{r})$  represent a periodic array of QDs [49–51] (see Fig. 5 in the Appendix), where the doped charge carriers (referred to, here, indiscriminately as ‘holes’) can be tightly bound.

In a superlattice with integer fillings [52, 53] and of a sufficiently large  $v_0$  (experimentally controlled), these Moiré attractive pockets behave as 2D isolated QDs, and the corresponding few-body problem (with  $N \leq 6$  holes, already experimentally realized [52, 53]), is the focus of this paper.

The isolated Moiré QD is evocative of the few-body problem in the electrostatically defined 2D semiconductor QDs. A major difference, however, exists between these two cases, readily grasped by expanding  $V(\mathbf{r})$  in Eq. (1) in powers of  $r$ , and defining a confining potential,  $V_{\text{MQD}}(\mathbf{r})$ , for the isolated Moiré QD as follows:

$$V_{\text{MQD}}(\mathbf{r}) \equiv V(\mathbf{r}) + 6v_0 \cos(\phi) \approx m^* \omega_0^2 r^2 / 2 + \mathcal{C} \sin(3\theta) r^3. \quad (2)$$

with  $m^* = 0.50m_e$  being the effective mass of the charge carriers,  $m^* \omega_0^2 = 16\pi^2 v_0 \cos(\phi) / a_M^2$ , and  $\mathcal{C} = 16\pi^3 v_0 \sin(\phi) / (3\sqrt{3}a_M^3)$ ; for the isolated Moiré QD, the expansion of  $V(\mathbf{r})$  can be restricted to the terms up to  $r^3$ . Because of the anisotropic second term, the  $V_{\text{MQD}}(\mathbf{r})$  confinement [Eq. (2)] has a  $C_3$  point-group symmetry and differs from that of a single circular 2D QD, which is well approximated solely by the harmonic term [first term in  $V_{\text{MQD}}(\mathbf{r})$  above]; the strength of the anisotropy is con-

\* Constantine.Yannouleas@physics.gatech.edu

† Uzi.Landman@physics.gatech.edu

trolled by the angle  $\phi$ . In the following, we analyze and illustrate the emergence of the counterintuitive behavior of the quantum WMs in this particular confinement. Specifically, our FCI results will show that a relatively weak  $\sin(3\theta)r^3$  term (case of  $\phi < 20^\circ$ ) can act as a pinning agent for the WM only in the case of  $N = 3$ , when the intrinsic WM azimuthal geometry [an empty-center (0,3) polygonal ring] coincides with the  $C_3$  point-group symmetry associated with  $\sin(3\theta)$ ; in this pinned case, the WM is visible in the charge density. In all other instances investigated here, however, there is no pinning [56], i.e., whilst the CDs preserve the  $C_3$  symmetry (as quantum-mechanically required), they do not exhibit any signature of Wigner molecularization. Unveiling (seeing) the hidden Wigner molecularization requires computation of the associated CPDs, which reveal the intrinsic  $(n_1, n_2)$  (with  $n_1 + n_2 = N$ ) concentric polygonal-ring configurations, familiar from the literature [10, 12, 14, 15, 17–19, 22–24, 26, 27, 33, 34] on circular 2D semiconductor QDs.

The Schrödinger equation for the many-body Hamiltonian of the isolated Moiré QD, given by

$$H_{\text{MB}} = \sum_{i=1}^N \left\{ \frac{\mathbf{p}_i^2}{2m^*} + V_{\text{MQD}}(\mathbf{r}_i) \right\} + \sum_{i<j}^N \frac{e^2}{\kappa|\mathbf{r}_i - \mathbf{r}_j|}, \quad (3)$$

is solved here using the aforementioned FCI methodology [17, 18, 23, 34, 41, 43–45], with the emergence of the Wigner molecularization analyzed using both the FCI CDs and CPDs;  $\kappa$  is the dielectric constant.

For values of  $\phi = 10^\circ$  and  $\phi = 30^\circ$ ,  $V_{\text{MQD}}(\mathbf{r})$  exhibits, respectively, weak and strong  $\sin(3\theta)r^3$  distortion away from the circular confinement; see Figs. 5(b) and 5(c) in the Appendix. We focus here on the  $\phi = 10^\circ$  case, with additional results for  $\phi = 30^\circ$  and  $\phi = 0$  presented in the Appendix (Figs. 6 and 7). Note, that the Wigner-molecularization propensity uncovered from the FCI results, is controlled by the Wigner parameter  $R_W = e^2/(\kappa l_0 \hbar \omega_0)$  [10, 23], expressing the ratio between the Coulomb repulsion and the quantum kinetic energy (proportional to the harmonic-oscillator energy gap);  $l_0 = [\hbar/(m^* \omega_0)]^{1/2}$  is the oscillator length. A high Wigner molecularization propensity is expected for  $R_W > 1$ .

Fig. 1 displays the CDs for  $N \leq 5$  in various characteristic instances when the holes are confined by the total  $V_{\text{MQD}}(\mathbf{r})$  potential with  $\phi = 10^\circ$ , except for the case of Fig. 1(II) when only the partial  $r^2$  term has been employed. In Fig. 1(I),  $\kappa = 1000$  was used to simulate the non-interacting limit, whereas  $\kappa = 5$  (strongly-interacting regime appropriate for the Moiré QD) was used in the rest of the frames.

The two frames for  $N = 2$  [with  $S = S_z = 0$ , Fig. 1(I) and Fig. 1(a)] demonstrate the effect of an increasing interparticle Coulomb repulsion (decreasing  $\kappa$ ) on the charge density. Indeed, in Fig. 1(I) (with  $\kappa = 1000$ , non-interacting regime) the CD is clearly associated with a doubly occupied  $1s$  orbital. In contrast, for  $\kappa = 5$  (Moiré-QD case), the  $N = 2$  charge density in Fig. 1(a) is spread

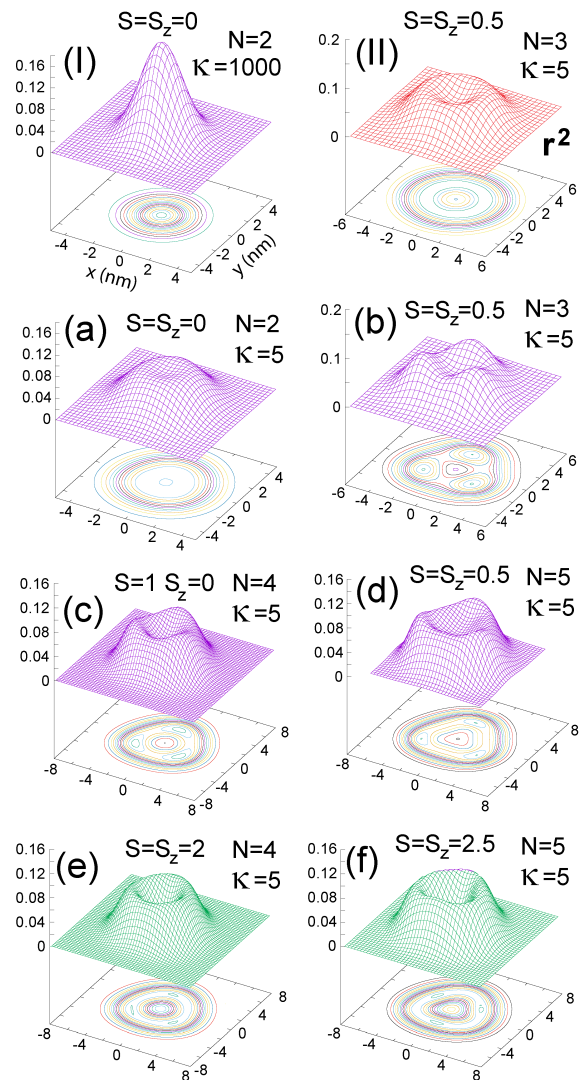


FIG. 1. FCI charge densities (normalized to  $N$ ) for  $N = 2 - 5$  holes in the isolated Moiré QD. In all frames:  $a_m = 14$  nm,  $m^* = 0.5m_e$ ,  $\phi = 10^\circ$ ,  $v_0 = 15$  meV, resulting in  $\hbar\omega_0 = 42.59073$  meV.  $\kappa = 5.0$  ( $R_W = 3.57$ ) except in frame (I), where  $\kappa = 1000$  ( $R_W = 0.018$ ) mimicks the non-interacting limit. In all cases, the total anisotropic confinement was considered, except in frame (II) (red-colored surface) where the confinement consists solely of the 2D circular harmonic contribution. The green color denotes fully polarized ( $S = S_z = N/2$ ) cases. A vanishing magnetic field,  $B = 0$ , was considered, except for  $N = 3$  and  $N = 5$  where a value of  $B = 1$  T was used in order to lift the ground-state degeneracy. All the remaining frames describe low-spin ground states. CDs in units of  $1/\text{nm}^2$ . See the text for a full description.

out over a considerably larger area and it assumes a ring-like shape by developing a depression at the origin. We note that this ring-like shape preserves the  $C_3$  symmetry of the total confining potential by being slightly deformed.

The CD in Fig. 1(a) does not exhibit the anticipated

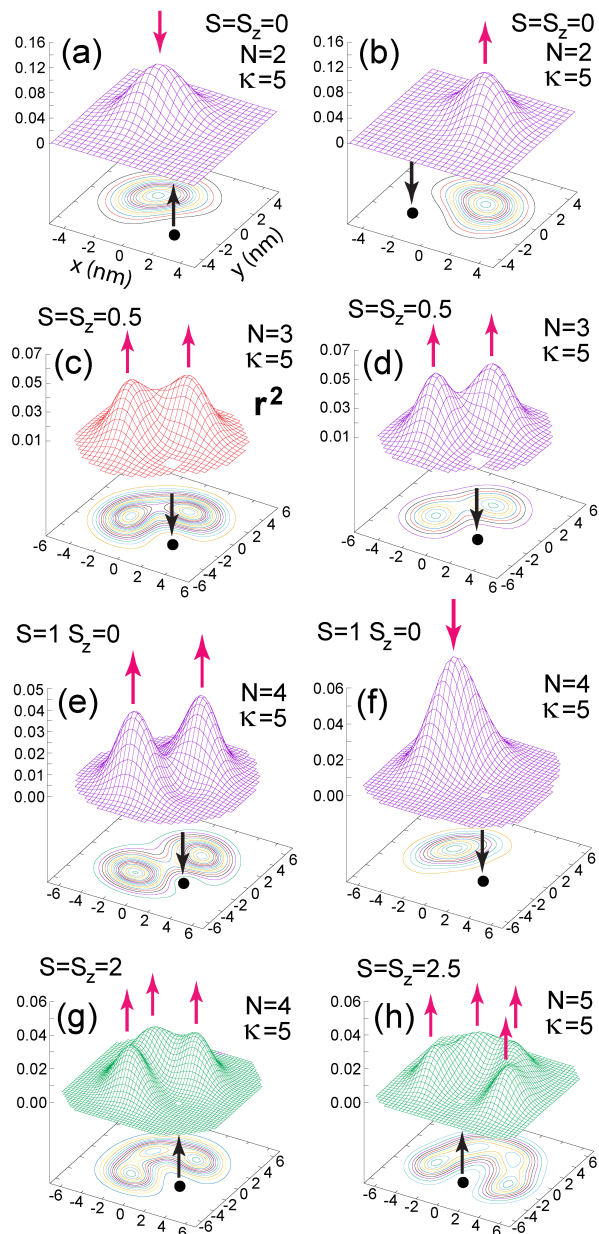


FIG. 2. FCI spin-resolved CPDs (normalized to unity) for  $N = 2 - 5$  holes in the isolated Moiré QD. Parameters (as denoted) are the same as in Fig. 1. In all cases, the total anisotropic confinement was considered, except in frame (c) (red-colored surface) where the confinement consists solely of the 2D circular harmonic contribution. The green color denotes again fully polarized ( $S = S_z = N/2$ ) cases, and all the remaining frames describe low-spin ground states. The black solid dot and black arrows denote the position and spin direction of the fixed-point fermions, respectively. The red arrows denote the positions (maxima of the spin surfaces) and spin direction of the remaining  $N - 1$  fermions. A vanishing magnetic field,  $B = 0$ , was considered, except for  $N = 3$  and  $N = 5$  where a value of  $B = 1$  T was used in order to lift the ground-state degeneracy. CPDs in units of  $1/nm^2$ . See the text for a full description.

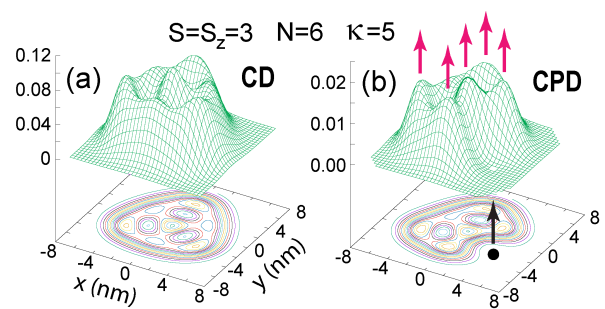


FIG. 3. FCI charge density (a) and spin-resolved CPD (b) for the lowest-in-energy fully spin-polarized state of  $N = 6$  holes in the isolated Moiré QD. The parameters  $a_M = 14$  nm,  $v_0 = 15$  meV,  $\phi = 10^\circ$ , and  $m^* = 0.5m_e$  are the same as in Fig. 1, and the dielectric constant  $\kappa = 5$  (yielding  $R_W = 3.57$ ). The full anisotropic confinement in Eq. (2) was considered here. The green color denotes again the fully polarized ( $S = S_z = 3$ ) case. The black solid dot and black arrow denote the position and spin direction of the fixed-point fermion, respectively. The red arrows denote the positions (maxima of the spin surface) and spin direction of the remaining 5 holes. A vanishing magnetic field,  $B = 0$ , was considered. See the text for a full description.

azimuthal geometry of a diatomic molecule, namely two localized particles in an antipodal arrangement. This WM configuration remains hidden in the charge density of Fig. 1(a), but it is revealed in the spin-resolved CPDs displayed in Fig. 2(a) and in Fig. 2(b). We note that in both cases of a fixed hole, with a spin up or a spin down, the second hole is found in an antipodal position with an opposite spin (spin down or spin up, respectively), as is consistent for a singlet state ( $S = S_z = 0$ ).

For  $N = 3$ , Fig. 1(II) and Fig. 1(b) exhibit a different behavior in the charge densities; this behavior also contrasts with that of the charge densities for all the remaining cases of  $N \leq 6$  holes investigated here. Specifically, when only the isotropic  $r^2$  potential term is retained in Eq. (2), the charge density is an azimuthally uniform ring [Fig. 1(II)]. However, further inclusion of the anisotropic  $\sin(3\theta)r^3$  term in the confining potential results in a drastic change in the charge density, which becomes that of three holes localized at the apices of an equilateral triangle [Fig. 1(b)]. One then can talk of a profoundly quantum, “rotating” (0,3) intrinsic WM polygonal-ring structure [57] in the case of Fig. 1(II), which transforms into a *pinned* WM in Fig. 1(b); the intrinsic (0,3) molecular structure is *unseen* in the charge density associated with the isotropic confinement [Fig. 1(II)], but it becomes visible in the spin-resolved CPD in Fig. 2(c). For completeness, we also display [Fig. 2(d)] the spin-resolved CPD for  $N = 3$  associated with the total potential, which is redundant, however, since, in this case, the (0,3) molecular configuration is already revealed in the charge density [Fig. 1(b)].

With the same parameters, the CDs for  $N = 4$  (left column) and  $N = 5$  (right column) are displayed in Fig.

1(c) and Fig. 1(d) for the ground states and in Fig. 1(e) and Fig. 1(f) for the lowest-in-energy fully spin-polarized states. All of these four densities preserve the  $C_3$  symmetry of the external confinement, but they are similar in shape and do not reveal any intrinsic molecular structure. Again, the intrinsic  $(0, N)$  polygonal configuration is revealed through the calculated FCI CPDs. In particular, two spin-resolved CPDs [spin-down at fixed-point, look for the two spin-ups, Fig. 2(e) and spin-down at fixed-point, look for the other spin-down, Fig. 2(f)], associated with the  $N = 4$  ground-state density of Fig. 1(c) are displayed in Fig. 2. Taking into account the two remaining CPDs (spin-up, look for spin-up and spin-up, look for spin-down, not shown), one sees that, in this particular case, the intrinsic spin eigenfunction of the rotating WM has the form  $(|\uparrow\downarrow\uparrow\downarrow\rangle - |\downarrow\uparrow\downarrow\uparrow\rangle)/\sqrt{2}$  [58], with the localized fermions arranged into a distorted  $(0,4)$  polygonal configuration. In the case of the fully polarized states in Fig. 2(g) ( $N = 4$ ) and Fig. 2(h) ( $N = 5$ ), there is only one spin-resolved CPD (spin-up, look for spin-up); in both cases this CPD reveals directly the intrinsic structure of a  $(0,4)$  and  $(0,5)$  polygonal WM. We note that the intrinsic polygonal configurations are necessarily slightly distorted in order to guarantee the  $C_3$  symmetry of the charge densities, because the CDs are equal to the integral of the CPDs over all possible positions of the fixed point.

We mention that the CD shapes (at  $\phi = 10^\circ$ ) presented here for  $2 \leq N \leq 4$  are in agreement with those displayed in Ref. [20] for a triangular semiconductor QD with an  $r^2 \cos(3\theta)$  anisotropy at a low magnetic field of  $B = 4$  T.

Fig. 3 demonstrates (for  $N = 6$ ) the case of a rotating WM with a more complex  $(1, N - 1)$  double-polygonal-intrinsic configuration. For simplicity (a single spin-resolved CPD), the lowest-in-energy fully spin-polarized state is considered. The FCI CD [Fig. 3(a)] preserves again the  $C_3$  confinement symmetry, but with a single fermion at the origin. In agreement, the CPD [Fig. 3(b)] reveals an  $(1,5)$  intrinsic WM geometry, with the outer polygonal ring containing five particles [59].

Using the FCI calculations for  $N = 2$ , we briefly discuss how the emergence of the Wigner molecularization negates the Aufbau principle that governs the natural atoms. Indeed, the ground-state for the non-interacting Moiré QD-Helium is approximated by an Aufbau-type single Slater determinant denoted as  $1s^2$ ; see Fig. 1(I). As shown in Fig. 4(a), the weight (%) of the  $1s^2$  Slater determinant in the FCI many-body wave function decreases drastically with decreasing  $\kappa$  (increasing correlations), and it vanishes for  $\kappa \rightarrow 0$ . In the charge-density plots, this behavior is associated with the developing of a depression at the origin (see Fig. 1(a) and Fig. 6 in the Appendix). For  $\kappa \rightarrow 0$ , singlet and triplet CDs coincide. Furthermore, in accordance, Fig. 4(b) demonstrates that the singlet-triplet energy gap [i.e., the gap  $\Delta_{\text{GLE}}$  between the ground state and the lowest excited one] decreases as well with decreasing  $\kappa$ , and it vanishes for  $\kappa \rightarrow 0$ . On the contrary, because  $N = 2$  is a 2D shell closure, the

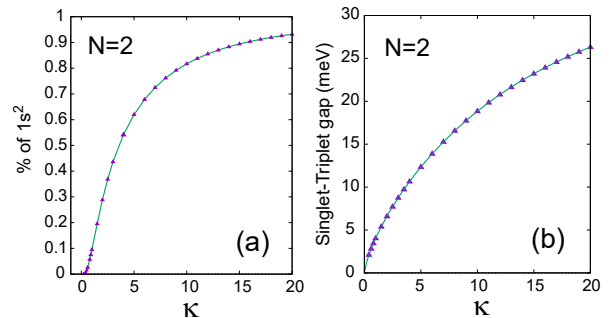


FIG. 4. (a) Weight (%) of the  $1s^2$  Slater determinant [an excellent approximation of the non-interacting ground state, see Fig. 1(I)] in the complete FCI wave function for  $N = 2$ , as a function of  $\kappa$ . (b) FCI singlet-triplet energy gap for  $N = 2$  as a function of  $\kappa$ . Remaining parameters:  $a_M = 14$  nm,  $v_0 = 15$  meV,  $\phi = 10^\circ$ , and  $m^* = 0.5m_e$ . See the text for a full description.

Aufbau approach would have yielded a value very close to the harmonic-oscillator gap,  $\hbar\omega_0$  (i.e., 42.59 meV for the parameters used in Fig. 4).

The voiding of the Aufbau principle with decreasing  $\kappa$  (increasing  $R_W$ ) can be also seen from the quenching of  $\Delta_{\text{GLE}}$  for  $N = 6$ , which is also a closed shell in the non-interacting limit. Indeed, for  $\kappa = 3$  and same other parameters as in Fig. 4, we find values of 1.68 meV, 2.50 meV, and 4.61 meV for the ( $S = 0 \rightarrow S = 2$ ), ( $S = 0 \rightarrow S = 1$ ), and ( $S = 0 \rightarrow S = 3$ ) gaps, respectively. These values are to be contrasted with the non-interacting  $\Delta_{\text{GLE}}$  of  $\approx \hbar\omega_0 = 42.59$  meV. This strong quenching of  $\Delta_{\text{GLE}}$ 's conforms with the expected full degeneracy of Wigner crystalline states belonging to a given total-spin multiplicity in the ‘‘classical’’ limit  $\kappa \rightarrow 0$  [60].

The FCI second differences,  $\Delta_2(N) = E(N + 1) + E(N - 1) - 2E(N)$ , associated with the ground-state energies, relate to the electrochemical potential gap  $\Delta\mu$  [61], which is experimentally accessible through measurements of the bilayer-sample capacitance [52]. With respect to the TMD bilayers, the  $\Delta_2(N)$  for the isolated QD relates to capacitance measurements at integer fillings  $\nu \geq 1$ . We found the FCI values:  $\Delta_2(2) = 93.55$  meV,  $\Delta_2(3) = 70.73$  meV,  $\Delta_2(4) = 78.06$  meV, and  $\Delta_2(5) = 60.34$  meV. These values suggest two FCI trends that are in general agreement with the results of Ref. [52]: (i) Due to the Wigner molecularization, the  $\Delta_2(N)$  values are substantially smaller than the corresponding Hubbard gap,  $U = e^2\sqrt{\pi}/(\kappa l_0) = 269.85$  meV, and (ii) on the average,  $\Delta_2(N)$  decreases with increasing  $N$  [62].

*Conclusions:* We show that the physics of quantum Wigner molecularization [10, 12, 14, 15, 17–19, 22–24, 26, 27, 33, 34], which goes beyond the Hubbard physics, underlies that of TMD Moiré superlattices at integer fillings  $\nu > 1$ , an artificial 2D material fast developing into a promising experimental platform [52, 53].

Our analysis, using both FCI CDs and CPDs for the single Moiré QD, demonstrates that the anisotropy of the Moiré confinement imposes an immediately visible  $C_3$  symmetry on the CDs, whilst the intrinsic polygonal-ring geometry of the WMs remains hidden and is revealed only using the CPDs. A notable exception is the case of  $N = 3$  charge carriers where, due to intrinsic and extrinsic symmetry coincidence, a pinned WM appears in the CD. Furthermore, due to the nature of WM correlations, the Moiré energy gaps are strongly quenched compared to both the predictions of the Hubbard model for strongly interacting systems and the Aufbau principle associated with the non-interacting case. Our results concerning the quantum WM phases can be experimentally verified using scanning tunneling microscopy for the CDs [49, 63] and scanning probe microscopy for the CPDs [64, 65].

This work has been supported by a grant from the Air Force Office of Scientific Research (AFOSR) under Award No. FA9550-21-1-0198. Calculations were carried out at the GATECH Center for Computational Materials Science.

**NOTE ADDED.** While completing this manuscript, we became aware of a recent arXiv eprint, D. Luo, A.P. Reddy, T. Devakul and L. Fu, “Artificial intelligence for artificial materials: moiré atom”, [arXiv:2303.08162v2](https://arxiv.org/abs/2303.08162v2) [66], where Wigner molecularization in isolated TMD Moiré QDs has been addressed. The results reported in that eprint differ substantially from our FCI results. We note in particular the inability of that study, based on neural network methodology, to (1) identify formation of a Wigner molecule for  $N = 2$ , and (2) recover the exact charge densities for  $N > 3$ . In the context of point (2) above, we call attention to pertinent remarks in Ref. [67] about ongoing issues pertaining to Wigner crystallization and fermionic neural networks.

## Appendix A: ILLUSTRATION OF THE TMD MOIRÉ POTENTIAL

Fig. 5 displays instances of the Moiré-superlattice potential given by Eq. (1) in the main text.

## Appendix B: THE CONFIGURATION INTERACTION METHOD

The full configuration interaction methodology has a long history, starting in quantum chemistry; see Refs. [41, 45]. The method was adapted to two dimensional problems and found extensive applications in the fields of semiconductor quantum dots [17, 18, 23, 34, 43, 44] and of the fractional quantum Hall effect [19, 68].

Our 2D FCI is described in our earlier publications. The reader will find a comprehensive exposition in Appendix B of Ref. [34], where the method was applied

to GaAs double-quantum-dot quantum computer qubits. The only difference with the present application to Moiré QDs, due to the different external confinement, concerns the space orbitals,  $\varphi_j(x, y)$ ,  $j = 1, 2, \dots, K$ , that are employed in the building of the spin-dependent, single-particle basis used to construct the Slater determinants  $\Psi_I^N$ , which span the many-body Hilbert space [see Eq. (B4) in Ref. [34]; the index  $I$  counts the Slater determinants]. Indeed, for a Moiré QD, the orbitals  $\varphi_j(x, y)$  are determined as solutions (in Cartesian coordinates) of the auxiliary Hamiltonian

$$H_{\text{aux}} = \frac{\mathbf{p}^2}{2m^*} + \frac{1}{2}m^*\omega_0^2(x^2 + y^2), \quad (\text{B1})$$

where  $m^*\omega_0^2 = 16\pi^2v_0 \cos(\phi)/a_M^2$ , i.e., only the isotropic parabolic (harmonic) contribution in  $V_{\text{MQD}}$  is included.

Following Ref. [34], we use a sparse-matrix eigensolver based on Implicitly Restarted Arnoldi methods (see ARPACK [69]) to diagonalize the many-body Hamiltonian in Eq. (3) of the main text. When a finite magnetic field  $B$  value is used, we replace  $\mathbf{p}$  by  $\mathbf{p} - (e/c)\mathbf{A}(\mathbf{r})$ , where the vector potential  $\mathbf{A}(\mathbf{r}) = 0.5B(-y, x)$  is taken according to the symmetric gauge.

The required one-body and two-body matrix elements for the ARPACK diagonalization are calculated as described in Ref. [34]. In addition, the matrix elements  $\langle \varphi_i(x, y) | \sin(3\theta)r^3 | \varphi_j(x, y) \rangle$  of the anisotropic term in the Moiré confinement are calculated analytically using the algebraic language MATHEMATICA [70] and the Hermite-to-Laguerre (Cartesian-to-polar) transformations listed in Ref. [71].

In all calculations, we used at a minimum values of  $K = 45$  and/or  $K = 55$ . For  $N = 2$  and  $N = 3$ , additional calculations were carried out employing an extended single-particle basis with  $K = 78$ . The maximum dimension of the many-body Hilbert space (the number of Slater determinants  $\Psi_I^N$  in the FCI expansion) reached a value of  $I_{\text{max}} \approx 5,000,000$  in some cases.

## Appendix C: CHARGE DENSITIES AND CONDITIONAL PROBABILITY DISTRIBUTIONS FROM FCI WAVE FUNCTIONS

The single-particle density (charge density) is the expectation value of a one-body operator

$$\rho(\mathbf{r}) = \langle \Phi_N^{\text{FCI}} | \sum_{i=1}^N \delta(\mathbf{r} - \mathbf{r}_i) | \Phi_N^{\text{FCI}} \rangle, \quad (\text{C1})$$

where  $\Phi_N^{\text{FCI}}$  denotes the many-body (multi-determinantal) FCI wave function, namely,

$$\Phi_N^{\text{FCI}}(\mathbf{r}_1, \dots, \mathbf{r}_N) = \sum_I C_I \Psi_I^N(\mathbf{r}_1, \dots, \mathbf{r}_N). \quad (\text{C2})$$

Naturally several distinct spin structures can correspond to the same charge density. The spin structure

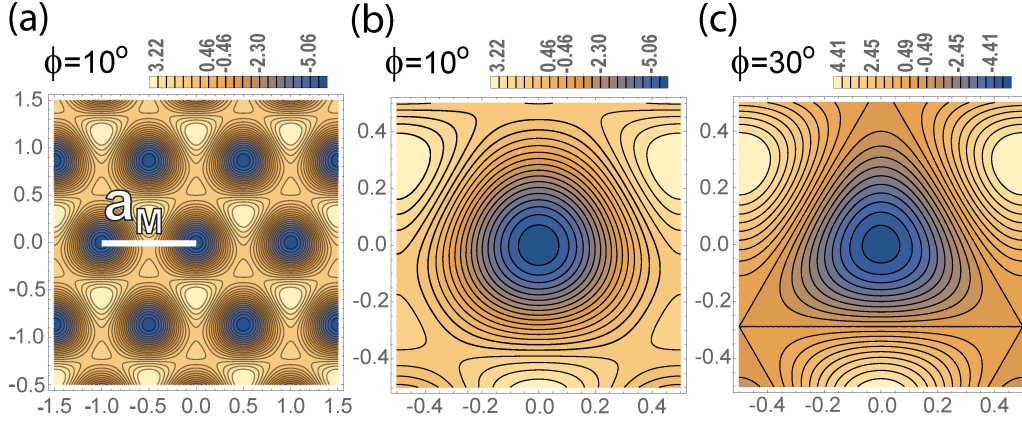


FIG. 5. Plot of the Moiré-superlattice potential given by Eq. (1) in the main text. (a) Broader view of the periodic potential structure for an angle of  $\phi = 10^\circ$ . (b) Potential of the isolated Moiré QD for  $\phi = 10^\circ$ . (c) Potential of the isolated Moiré QD for  $\phi = 30^\circ$ . Lengths in units of the Moiré lattice constant  $a_M$ . Potential contours in units of  $v_0$ .

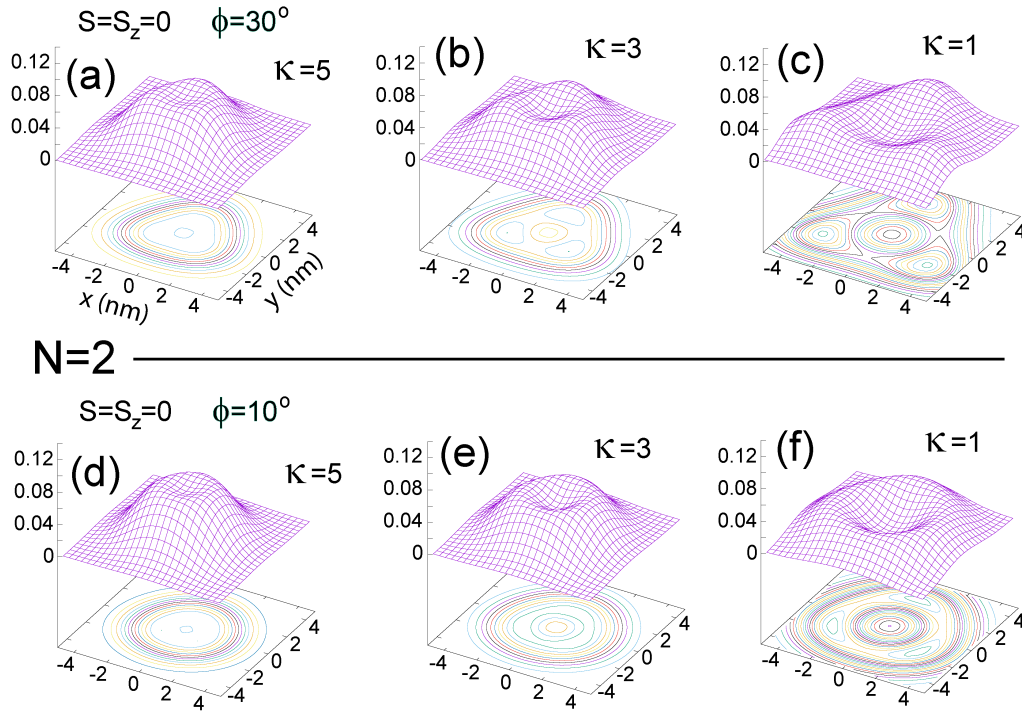


FIG. 6. FCI Moiré-QD charge densities [i.e., for the total potential,  $V_{\text{MQD}}$ , in Eq. (2) of the main text which includes both the harmonic and cubic contributions] for the singlet state of  $N = 2$  holes, and for different values of the dielectric constant  $\kappa$  and the  $\phi$ -angle. Remaining parameters used:  $a_M = 14$  nm,  $v_0 = 15$  meV,  $m^* = 0.5m_e$ . (a-c)  $\phi = 30^\circ$ . (d-f)  $\phi = 10^\circ$ . Left column:  $\kappa = 5$ . Middle column:  $\kappa = 3$ . Right column:  $\kappa = 1$ . The corresponding Wigner parameter ( $R_W$ ) values are: (a) 3.69, (b) 6.15, (c) 18.46, (d) 3.57, (e) 5.95, and (f) 17.85. The progressive enhancement of the depression at the origin as a function of decreasing  $\kappa$  (increasing  $R_W$ ) is clearly seen for the cases of both angles  $\phi$ . These ring-like charge densities correspond to a rotating Wigner molecule whose intrinsic geometric configuration [denoted by (0,2)] consists of two antipodal fermions; see main text. CDs in units of  $1/\text{nm}^2$ .

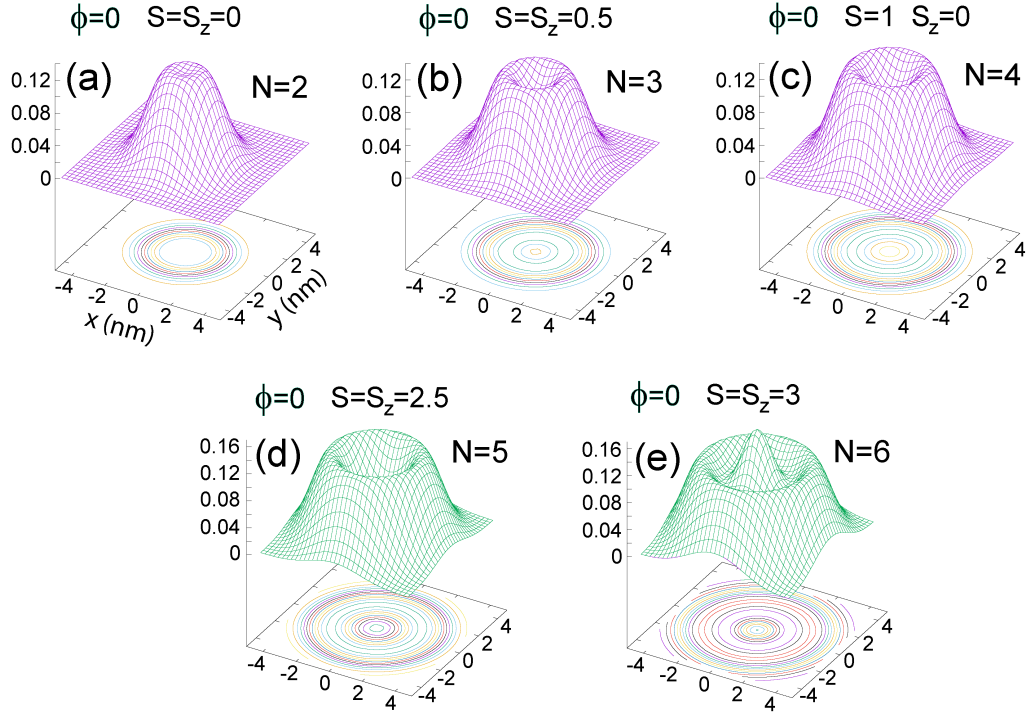


FIG. 7. FCI Moiré-QD, charge densities for the total potential,  $V_{\text{MQD}}$ , [Eq. (2) of the main text] for a vanishing angle  $\phi = 0^\circ$ . In this case only the harmonic term in the expansion survives, and the confinement has circular symmetry. (a) ground-state CD for  $N = 2$  holes. (b) ground-state CD for  $N = 3$  holes. (c) ground-state CD for  $N = 4$  holes. (d,e) CDs of the lowest-in-energy fully spin-polarized states for  $N = 5$  and  $N = 6$  holes, respectively. The remaining parameters are:  $a_M = 15$  nm,  $v_0 = 20$  meV,  $m^* = 1 m_e$ , and  $\kappa = 10$ , which yields  $R_W = 2.88$ . These uniform, ring-like charge densities correspond to a rotating Wigner molecule whose intrinsic geometric configuration [denoted as  $(0, N)$  or  $(1, N - 1)$ ] consists of regular polygons with the particles being localized at the apices of the polygons. The results in this figure are in full agreement with the previous abundant literature on 2D semiconductor quantum dots; see Ref. [23] and references therein. CDs in units of  $1/\text{nm}^2$ .

associated with a specific FCI wave function can be determined with the help of the many-body spin-resolved CPDs [12, 19, 22, 23, 29, 54].

The spin-resolved CPDs yield the conditional probability distribution of finding another fermion with up (or down) spin  $\sigma$  at a position  $\mathbf{r}$ , assuming that a given fermion with up (or down) spin  $\sigma_0$  is fixed at  $\mathbf{r}_0$ . Specifically, the spin-resolved two-point anisotropic correlation function is defined as the the expectation value of a two-body operator

$$P_{\sigma\sigma_0}(\mathbf{r}, \mathbf{r}_0) = \langle \Phi_N^{\text{FCI}} | \sum_{i \neq j} \delta(\mathbf{r} - \mathbf{r}_i) \delta(\mathbf{r}_0 - \mathbf{r}_j) \delta_{\sigma\sigma_i} \delta_{\sigma_0\sigma_j} | \Phi_N^{\text{FCI}} \rangle. \quad (\text{C3})$$

Using a normalization constant

$$\mathcal{N}(\sigma, \sigma_0, \mathbf{r}_0) = \int P_{\sigma\sigma_0}(\mathbf{r}, \mathbf{r}_0) d\mathbf{r}, \quad (\text{C4})$$

we define a related conditional probability distribution (CPD) as

$$\mathcal{P}_{\sigma\sigma_0}(\mathbf{r}, \mathbf{r}_0) = P_{\sigma\sigma_0}(\mathbf{r}, \mathbf{r}_0) / \mathcal{N}(\sigma, \sigma_0, \mathbf{r}_0), \quad (\text{C5})$$

having the property  $\int \mathcal{P}_{\sigma\sigma_0}(\mathbf{r}, \mathbf{r}_0) d\mathbf{r} = 1$ .

#### Appendix D: ADDITIONAL CHARGE DENSITIES

In this part, we present additional charge densities for parameters, different from those used in the main text; see Fig. 6 and Fig. 7. In addition to the angle value of  $\phi = 10^\circ$ , charge densities for the values of  $\phi = 30^\circ$  and  $\phi = 0^\circ$  are presented.

[1] M. Jammer, *The philosophy of quantum mechanics* (Wiley, New York, 1974).

[2] A. Pais, *Niels Bohr's Times, In Physics, Philosophy, and Polity* (Oxford University Press, Oxford, 1991).

- [3] L. P. Kouwenhoven, C. M. Marcus, P. L. McEuen, S. Tarucha, R. M. Westervelt, and N. S. Wingreen, Electron transport in quantum dots, in *Mesoscopic Electron Transport*, edited by L. L. Sohn, L. P. Kouwenhoven, G. Schön (Springer Netherlands, Dordrecht, 1997) p. 105.
- [4] R. Hanson, L. P. Kouwenhoven, J. R. Petta, S. Tarucha, and L. M. K. Vandersypen, Spins in few-electron quantum dots, *Rev. Mod. Phys.* **79**, 1217–1265 (2007).
- [5] F.-M. Jing, Z.-Z. Zhang, G.-Q. Qin, G. Luo, G. Cao, H.-O. Li, X.-X. Song, and G.-P. Guo, Gate-controlled quantum dots based on 2D materials, *Advanced Quantum Technologies* **5**, 2100162 (2022).
- [6] F. A. Zwanenburg, A. S. Dzurak, A. Morello, M. Y. Simmons, L. C. L. Hollenberg, G. Klimeck, S. Rogge, S. N. Coppersmith, and M. A. Eriksson, Silicon quantum electronics, *Rev. Mod. Phys.* **85**, 961–1019 (2013).
- [7] L. M. K. Vandersypen and M. A. Eriksson, Quantum computing with semiconductor spins, *Phys. Today* **72**, 38–45 (2019).
- [8] G.-W. Deng, N. Xu, and W.-J. Li, Gate-defined quantum dots: Fundamentals and applications, in *Quantum Dot Optoelectronic Devices*, edited by P. Yu and Z. M. Wang (Springer International Publishing, Cham, 2020) pp. 107–133.
- [9] G. Burkard, T. D. Ladd, J. M. Nichol, A. Pan, and J. R. Petta, Semiconductor Spin Qubits, [arXiv:2112.08863](https://arxiv.org/abs/2112.08863).
- [10] C. Yannouleas and U. Landman, Spontaneous Symmetry Breaking in Single and Molecular Quantum Dots, *Phys. Rev. Lett.* **82**, 5325–5328 (1999).
- [11] R. Egger, W. Häusler, C. H. Mak, and H. Grabert, Crossover from Fermi liquid to Wigner molecule behavior in quantum dots, *Phys. Rev. Lett.* **82**, 3320–3323 (1999).
- [12] C. Yannouleas and U. Landman, Collective and Independent-Particle Motion in Two-Electron Artificial Atoms, *Phys. Rev. Lett.* **85**, 1726–1729 (2000).
- [13] A. V. Filinov, M. Bonitz, and Y. E. Lozovik, Wigner Crystallization in Mesoscopic 2D Electron Systems, *Phys. Rev. Lett.* **86**, 3851–3854 (2001).
- [14] C. Yannouleas and U. Landman, Strongly correlated wavefunctions for artificial atoms and molecules, *Journal of Physics: Condensed Matter* **14**, L591–L598 (2002).
- [15] S. A. Mikhailov, Two ground-state modifications of quantum-dot beryllium, *Phys. Rev. B* **66**, 153313 (2002).
- [16] A. Harju, S. Siljamäki, and R. M. Nieminen, Wigner molecules in quantum dots: A quantum monte carlo study, *Phys. Rev. B* **65**, 075309 (2002).
- [17] C. Yannouleas and U. Landman, Two-dimensional quantum dots in high magnetic fields: Rotating-electron-molecule versus composite-fermion approach, *Phys. Rev. B* **68**, 035326 (2003).
- [18] M. B. Tavernier, E. Anisimovas, F. M. Peeters, B. Szafran, J. Adamowski, and S. Bednarek, Four-electron quantum dot in a magnetic field, *Phys. Rev. B* **68**, 205305 (2003).
- [19] C. Yannouleas and U. Landman, Structural properties of electrons in quantum dots in high magnetic fields: Crystalline character of cusp states and excitation spectra, *Phys. Rev. B* **70**, 235319 (2004).
- [20] B. Szafran, F. M. Peeters, S. Bednarek, and J. Adamowski, Anisotropic quantum dots: Correspondence between quantum and classical Wigner molecules, parity symmetry, and broken-symmetry states, *Phys. Rev. B* **69**, 125344 (2004).
- [21] I. Romanovsky, C. Yannouleas, L. O. Baksmaty, and U. Landman, Bosonic molecules in rotating traps, *Phys. Rev. Lett.* **97**, 090401 (2006).
- [22] Y. Li, C. Yannouleas, and U. Landman, From a few to many electrons in quantum dots under strong magnetic fields: Properties of rotating electron molecules with multiple rings, *Phys. Rev. B* **73**, 075301 (2006).
- [23] C. Yannouleas and U. Landman, Symmetry breaking and quantum correlations in finite systems: Studies of quantum dots and ultracold Bose gases and related nuclear and chemical methods, *Reports on Progress in Physics* **70**, 2067–2148 (2007).
- [24] Z. Dai, J.-L. Zhu, N. Yang, and Y. Wang, Spin-dependent rotating Wigner molecules in quantum dots, *Phys. Rev. B* **76**, 085308 (2007).
- [25] L. O. Baksmaty, C. Yannouleas, and U. Landman, Rapidly rotating boson molecules with long- or short-range repulsion: An exact diagonalization study, *Phys. Rev. A* **75**, 023620 (2007).
- [26] A. Ghosal, A. D. Güçlü, C. J. Umrigar, D. Ullmo, and H. U. Baranger, Incipient Wigner localization in circular quantum dots, *Phys. Rev. B* **76**, 085341 (2007).
- [27] N. Yang, J.-L. Zhu, and Z. Dai, Rotating Wigner molecules and spin-related behaviors in quantum rings, *Journal of Physics: Condensed Matter* **20**, 295202 (2008).
- [28] I. Romanovsky, C. Yannouleas, and U. Landman, Edge states in graphene quantum dots: Fractional quantum Hall effect analogies and differences at zero magnetic field, *Phys. Rev. B* **79**, 075311 (2009).
- [29] B. B. Brandt, C. Yannouleas, and U. Landman, Double-well ultracold-fermions computational microscopy: Wave-function anatomy of attractive-pairing and Wigner-molecule entanglement and natural orbitals, *Nano Letters* **15**, 7105–7111 (2015).
- [30] C. Yannouleas and U. Landman, Exact closed-form analytic wave functions in two dimensions: Contact-interacting fermionic spinful ultracold atoms in a rapidly rotating trap, *Phys. Rev. Research* **3**, L032028 (2021).
- [31] H. E. Ercan, S. N. Coppersmith, and M. Friesen, Strong electron-electron interactions in Si/SiGe quantum dots, *Phys. Rev. B* **104**, 235302 (2021).
- [32] J. C. Abadillo-Uriel, B. Martinez, M. Filippone, and Y.-M. Niquet, Two-body Wigner molecularization in asymmetric quantum dot spin qubits, *Phys. Rev. B* **104**, 195305 (2021).
- [33] C. Yannouleas and U. Landman, Wigner molecules and hybrid qubits, *J. Phys.: Condens. Matter (Letter)* **34**, 21LT01 (2022).
- [34] C. Yannouleas and U. Landman, Molecular formations and spectra due to electron correlations in three-electron hybrid double-well qubits, *Phys. Rev. B* **105**, 205302 (2022).
- [35] C. Ellenberger, T. Ihn, C. Yannouleas, U. Landman, K. Ensslin, D. Driscoll, and A. C. Gossard, Excitation Spectrum of Two Correlated Electrons in a Lateral Quantum Dot with Negligible Zeeman Splitting, *Phys. Rev. Lett.* **96**, 126806 (2006).
- [36] S. Kalliakos, M. Rontani, V. Pellegrini, C. P. García, A. Pinczuk, G. Goldoni, E. Molinari, L. N. Pfeiffer, and K. W. West, A molecular state of correlated electrons in a quantum dot, *Nature Physics* **4**, 467–471 (2008).
- [37] W. Jang, M.-K. Cho, H. Jang, J. Kim, J. Park, G. Kim, B. Kang, H. Jung, V. Umansky, and D. Kim, Single-Shot Readout of a Driven Hybrid Qubit in a GaAs Double

- Quantum Dot, *Nano Letters* **21**, 4999–5005 (2021).
- [38] W. Jang, J. Kim, J. Park, G. Kim, M.-K. Cho, H. Jang, S. Sim, B. Kang, H. Jung, V. Umansky, and D. Kim, Wigner-molecularization-enabled dynamic nuclear field programming, [arXiv:2207.11655](https://arxiv.org/abs/2207.11655).
- [39] J. Corrigan, J. P. Dodson, H. E. Ercan, J. C. Abadillo-Uriel, B. Thorgrimsson, T. J. Knapp, N. Holman, T. McJunkin, S. F. Neyens, E. R. MacQuarrie, R. H. Foote, L. F. Edge, M. Friesen, S. N. Coppersmith, and M. A. Eriksson, Coherent control and spectroscopy of a semiconductor quantum dot Wigner molecule, *Phys. Rev. Lett.* **127**, 127701 (2021).
- [40] S. Pecker, F. Kuemmeth, A. Secchi, M. Rontani, D. C. Ralph, P. L. McEuen, and S. Ilani, Observation and spectroscopy of a two-electron Wigner molecule in an ultraclean carbon nanotube, *Nature Physics* **9**, 576–581 (2013).
- [41] I. Shavitt, The history and evolution of configuration interaction, *Molecular Physics* **94**, 3–17 (1998).
- [42] C. Yannouleas and U. Landman, Electron and boson clusters in confined geometries: Symmetry breaking in quantum dots and harmonic traps, *Proceedings of the National Academy of Sciences* **103**, 10600–10605 (2006).
- [43] M. Rontani, C. Cavazzoni, D. Bellucci, and G. Goldoni, Full configuration interaction approach to the few-electron problem in artificial atoms, *The Journal of Chemical Physics* **124**, 124102 (2006).
- [44] C. Yannouleas and U. Landman, Valleytronic full configuration-interaction approach: Application to the excitation spectra of si double-dot qubits, *Phys. Rev. B* **106**, 195306 (2022).
- [45] A. Szabo and N. S. Ostlund, *Modern Quantum Chemistry* (McGraw-Hill, New York, 1989) For the Slater-Condon rules, see Chap. 4.
- [46] V. N. Ostrovsky, What and how physics contributes to understanding the periodic law, *Foundations of Chemistry* **3**, 145–181 (2001).
- [47] J. Hubbard and B. H. Flowers, Electron correlations in narrow energy bands, *Proceedings of the Royal Society of London. Series A. Mathematical and Physical Sciences* **276**, 238–257 (1963).
- [48] J. Hubbard, Generalized Wigner lattices in one dimension and some applications to tetracyanoquinodimethane (TCNQ) salts, *Phys. Rev. B* **17**, 494–505 (1978).
- [49] Y. Pan, S. Fölsch, Y. Nie, D. Waters, Y.-C. Lin, B. Jariwala, K. Zhang, K. Cho, J. A. Robinson, and R. M. Feenstra, Quantum-confined electronic states arising from the Moiré pattern of MoS<sub>2</sub>-WSe<sub>2</sub> heterobilayers, *Nano Letters* **18**, 1849–1855 (2018), <https://doi.org/10.1021/acs.nanolett.7b05125>.
- [50] Y. Zeng and A. H. MacDonald, Strong modulation limit of excitons and trions in Moiré materials, *Phys. Rev. B* **106**, 035115 (2022).
- [51] Z. Song, Y. Wang, H. Zheng, P. Narang, and L.-W. Wang, Deep quantum-dot arrays in Moiré superlattices of non-van der Waals materials, *Journal of the American Chemical Society* **144**, 14657–14667 (2022).
- [52] T. Li, J. Zhu, Y. Tang, K. Watanabe, T. Taniguchi, V. Elser, J. Shan, and K. F. Mak, Charge-order-enhanced capacitance in semiconductor Moiré superlattices, *Nature Nanotechnology* **16**, 1068–1072 (2021).
- [53] B. A. Foutty, J. Yu, T. Devakul, C. R. Kometter, Y. Zhang, K. Watanabe, T. Taniguchi, L. Fu, and B. E. Feldman, Tunable spin and valley excitations of correlated insulators in  $\Gamma$ -valley Moiré bands, [arXiv:2206.10631](https://arxiv.org/abs/2206.10631).
- [54] Y. Li, C. Yannouleas, and U. Landman, Artificial quantum-dot Helium molecules: Electronic spectra, spin structures, and Heisenberg clusters, *Phys. Rev. B* **80**, 045326 (2009).
- [55] F. Wu, T. Lovorn, E. Tutuc, and A. H. MacDonald, Hubbard model physics in transition metal dichalcogenide Moiré bands, *Phys. Rev. Lett.* **121**, 026402 (2018).
- [56] Our findings concerning the prerequisites for WM pinning agree with the results in T. Chwiej and B. Szafran, Pinning of electron densities in quantum rings by defects: Symmetry constraints and distribution of persistent currents, *Phys. Rev. B* **79**, 085305 (2009).
- [57] Indeed, the term “rotating Wigner (or electron) molecule” has been used to accentuate the quantum nature of the Wigner molecule in earlier literature; see, e.g., Refs. [17, 19, 22–24, 27].
- [58] For the complete set of possible  $N = 4$  spin eigenfunctions, see Ref. [54], and references therein.
- [59] The subtle interplay discussed here between the *symmetry-preserving* exact CDs and the apparently *symmetry-breaking* intrinsic WM configurations has been noted and discussed in earlier literature; see Ref. [23], and references therein, Ref. [14], and J. A. Sheikh, J. Dobaczewski, P. Ring, L. M. Robledo, and C. Yannouleas, Symmetry restoration in mean-field approaches, *Journal of Physics G: Nuclear and Particle Physics* **48**, 123001 (2021), and references therein
- [60] A similar degeneracy happens also for contact interaction; see C. Yannouleas, B. B. Brandt, and U. Landman, Ultracold few fermionic atoms in needle-shaped double wells: spin chains and resonating spin clusters from microscopic Hamiltonians emulated via antiferromagnetic Heisenberg and  $t - J$  models, *New Journal of Physics* **18**, 073018 (2016).
- [61] L. P. Kouwenhoven, N. C. van der Vaart, A. T. Johnson, W. Kool, C. J. P. M. Harmans, J. G. Williamson, A. A. M. Staring, and C. T. Foxon, Single electron charging effects in semiconductor quantum dots, *Zeitschrift für Physik B: Condensed Matter* **85**, 367–373 (1991).
- [62] The  $\nu$  assignments in Ref. [52] correspond to  $N - 1$  here.
- [63] H. Li, S. Li, E. C. Regan, D. Wang, W. Zhao, S. Kahn, K. Yumigeta, M. Blei, T. Taniguchi, K. Watanabe, S. Tongay, A. Zettl, M. F. Crommie, and F. Wang, Imaging two-dimensional generalized Wigner crystals, *Nature* **597**, 650–654 (2021).
- [64] E. Wach, D. P. Żebrowski, and B. Szafran, Charge density mapping of strongly-correlated few-electron two-dimensional quantum dots by the scanning probe technique, *Journal of Physics: Condensed Matter* **25**, 335801 (2013).
- [65] M. A. Topinka, B. J. LeRoy, S. E. J. Shaw, E. J. Heller, R. M. Westervelt, K. D. Maranowski, and A. C. Gossard, Imaging coherent electron flow from a quantum point contact, *Science* **289**, 2323–2326 (2000).
- [66] D. Luo, A. P. Reddy, T. Devakul, and L. Fu, Artificial intelligence for artificial materials: Moiré atom, [arXiv:2303.08162](https://arxiv.org/abs/2303.08162).
- [67] G. Cassella, H. Sutterud, S. Azadi, N. D. Drummond, D. Pfau, J. S. Spencer, and W. M. C. Foulkes, Discovering Quantum Phase Transitions with Fermionic Neural Networks, *Phys. Rev. Lett.* **130**, 036401 (2023).

- [68] J. K. Jain, *Composite Fermions* (Cambridge University Press, Cambridge, 2007).
- [69] R. B. Lehoucq, D. C. Sorensen, and C. Yang, *ARPACK USERS' GUIDE: Solution of Large-Scale Eigenvalue Problems with Implicitly Restarted ARNOLDI Methods* (SIAM, Philadelphia, 1998).
- [70] Wolfram Research, Inc., [Mathematica, Version 13.2](#), Champaign, IL, 2022.
- [71] I. Kimel and L. Elias, Relations between Hermite and Laguerre Gaussian modes, [IEEE Journal of Quantum Electronics](#) **29**, 2562–2567 (1993).